TECHNICAL PAPER

Lateral control strategy based on head movement responses for motion sickness mitigation in autonomous vehicle

Sarah 'Atifah Saruchi[1] · Mohd Hatta Mohammed Ariff[1] · Hairi Zamzuri[1,2] · Noor Hafizah Amer[3] · Nurbaiti Wahid[4] · Nurhaffizah Hassan[4] · Zulkiffli Abdul Kadir[3]

Abstract

Passengers are more susceptible to motion sickness (MS) than the drivers because during cornering, they tilt their heads according to lateral acceleration direction, while the drivers tilt their heads against it. During slalom driving, high lateral acceleration that resulted from inappropriate wheel's turning will increase the severity level of MS as it contributes to a larger passenger's head roll angle towards the lateral acceleration direction. Thus, for an autonomous vehicle, it is necessary to design a smooth lateral control to obtain appropriate wheel angle to prevent high lateral acceleration. This study proposes an inner-loop lateral control strategy which utilized head roll angle as the controlled variable to generate corrective wheel angle to reduce the lateral acceleration. Firstly, an estimation model of driver's and passenger's head roll angle is developed by radial basis function network method based on the correlation between lateral acceleration and occupant's head roll angle. The driver's and passenger's models are considered as the reference and the controlled subject, respectively. Secondly, a fuzzy logic controller is adopted to generate corrective wheel angle based on the head roll angle responses. The reduction of the lateral acceleration caused by the corrective wheel angle minimized the passenger's head roll angle and hence mitigated their MS level. Simulation results show 3.25% and 10.86% reduction of motion sickness incidence in a single lap and ten laps after the proposed control strategy is applied. It is expected that the proposed control strategy will contribute to the MS mitigation study in autonomous vehicle field.

Keywords Autonomous vehicle · Lateral control · Motion sickness · Fuzzy logic controller · Radial basis function network

1 Introduction

Autonomous vehicle is a part of continuing evolution in automotive technology which received considerable attention among researchers because it brings potential benefits to the transportation system in terms of safety, mobility and environment [1]. Despite drawing a lot of attention, there is a challenge that leads to a significantly negative impact to the passenger's comfort during the automated driving which is called motion sickness (MS). It is an unpleasant condition commonly faced by the passengers who are travelling by car, train, air and particularly sea [2]. Generally, the wide range of signs and symptoms of MS includes sweating, salivation, dizziness, nausea, vomiting and other physical discomfort [3–5].

It is a well-known fact that the passenger is more prone to experience MS compared to the driver. Studies revealed that the head movement tilting direction differences between the passengers and the driver towards the lateral acceleration direction during curve driving contribute to the different amount of MS [6–9]. As shown in Fig. 1, when negotiating a curve, passengers normally tend to tilt their heads towards the lateral acceleration direction, while the driver tilts his/ her head in the opposite direction. The correlation between

✉ Mohd Hatta Mohammed Ariff
mohdhatta.kl@utm.my

1 Malaysia-Japan International Institute of Technology, University Technology Malaysia, 54000 Kuala Lumpur, Malaysia

2 Emoovit Technology Sdn. Bhd, Futurise Centre, 63000 Cyberjaya, Selangor, Malaysia

3 Faculty of Engineering, Universiti Pertahanan Nasional Malaysia, 57000 Kuala Lumpur, Malaysia

4 Faculty of Electrical Engineering, Universiti Teknologi Mara, 23000 Dungun, Malaysia
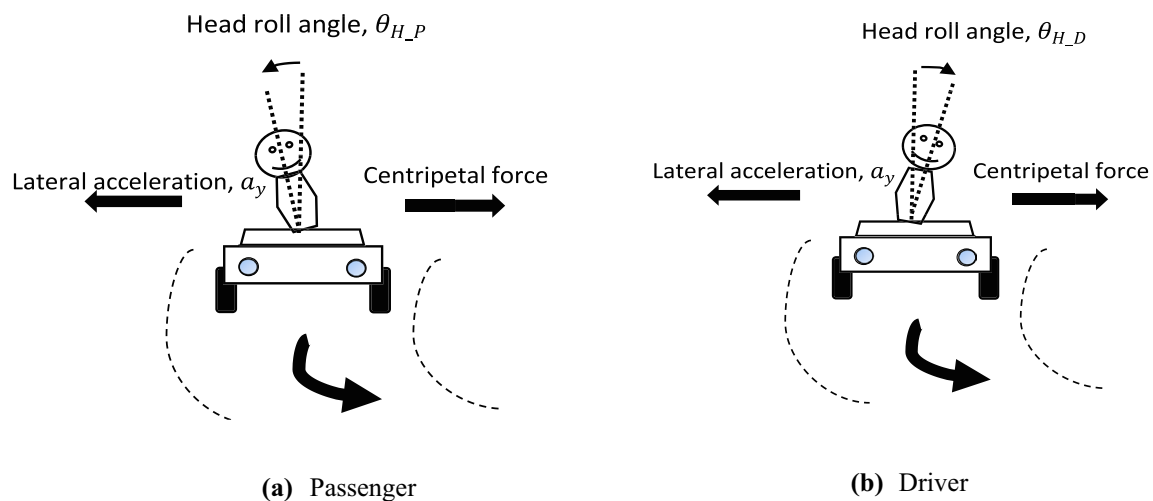
(a) Passenger

(b) Driver

Fig. 1 Typical occupant's head movement during cornering

the head tilt movement and the vehicle lateral acceleration leads to an easier effort for MS mitigation study. Based on the correlation, the higher the lateral acceleration, the larger the passenger's head roll angle will become. In this situation, the passenger's MS level will be increased. On the other hand, the passenger's head roll angle will become smaller when the lateral acceleration is lower. It will cause a reduction in the passenger's susceptibility towards MS. The passenger can also minimize their MS by imitating the driver's head tilt movement which is opposite to the lateral acceleration direction.

The relationship between lateral acceleration and MS is further supported by the research works done by Turner et al. [10]. MS occurs in low frequency of lateral acceleration (0.1–0.5 Hz) environment, and its effects increased as a function of duration of exposure and the intensity of acceleration. The author also stated that the primary cause of the MS increment is due to the high lateral acceleration resulted from the driver's turning method. Thus, it means that a smooth wheel control when dealing with curvatures can reduce the MS level [11]. It is easier to implement the wheel control strategy in autonomous vehicle rather than the conventional vehicle because there is no involvement of the driver's steering behaviour which is known to be specific and hard to control [12]. From the above statement, it can be concluded that one of the origins of the passenger's MS from vehicle dynamic perspective is the inappropriate wheel control. Combining the factors of MS occurrence in terms of passenger's behaviour and vehicle dynamic perspectives, it can be concluded that inappropriate wheel turning produced higher lateral acceleration which will cause larger passenger's head roll angle towards the lateral acceleration direction. This situation will lead to a bigger percentage of MS level.

Aiming to avoid inappropriate wheel input to the autonomous vehicle, the main contribution of this study is the proposal of a lateral control strategy with head roll angle as the controlled variable in order to generate an additional corrective wheel angle. The objective of the control structure is to reduce the lateral acceleration as well as the passenger's head roll angle so that the MS level can be minimized. The uniqueness of the structure is by introducing head roll angle as the controlled variable to generate corrective wheel angle instead of using well-known variables such as yaw rate and body slip as per presented in [13, 14]. As mentioned earlier, driver faced less MS because he/she tends to tilt their head against the lateral acceleration direction. Thus, the driver's head tilt response is assumed as the reference response. Besides, the passenger's head tilt response is considered as the actual controlled subject. Based on the error of the desired and the actual head roll angles, a corrective wheel angle is computed using a controller. Here, fuzzy logic controller (FLC) is adopted to play the role. It is one of the effective techniques to be used in nonlinear dynamic system [15]. The main feature of FLC is that it can be implemented without defining the controlled plant mathematically [16, 17]. For comparative analysis purposes, the performance of FLC is compared to the well-known proportional–integral–derivative (PID) controller. The proposed control system is simulated via Matlab/Simulink software. The limitation of this study is that it is merely conducted in simulation platform.

In the control structure design, there is a non-negligible issue that needs to be solved. Problem had arisen due to unknown exact values or quantities of the passenger's and the driver's head roll angles towards and against the lateral acceleration direction during cornering. The usage of head roll motion sensors all the time during travelling is believed

to be unpractical. Hence, it is necessary to establish models which can estimate the driver's and passenger's head roll angle. Here, the prediction models are developed using radial basis function network (RBFN) method based on the correlation between the occupant's head roll and the vehicle's lateral acceleration direction. Previously, the model had been developed by using system identification (SI) method [18, 19]. Other than SI, artificial neural network (ANN) and time delay neural network (TDNN) had also been used to model the correlation [20, 21]. Compared to the statistical models, neural network (NN) does not require any simplifying assumptions or prior knowledge of problem solving [22]. Rather than backpropagation neural network (BPNN), generalized regression neural network (GRNN) and multi-layer perception neural network (MLPNN), it has been reported that RBFN has better approximation performance and simpler structure and requires less training time [22–24].

2 Vehicle model and its path tracking system

2.1 Vehicle system model

As shown in Fig. 2, the current study implemented a 7-DOF nonlinear vehicle model as the vehicle plant for the suggested control approach. Table 1 gives the parameter of the vehicle system. The governing equations of the longitudinal, lateral and yaw motions are expressed as [25]:

$$m(\dot{v}_x - v_y\gamma) = (F_{xFL} + F_{xFR})\cos\delta - (F_{yFL} + F_{yFR})\sin\delta + F_{xRL} + F_{xRR} \tag{1}$$

$$m(\dot{v}_y + v_x\gamma) = (F_{yFL} + F_{yFR})\cos\delta + (F_{xFL} + F_{xFR})\sin\delta + F_{yRL} + F_{yRR} \tag{2}$$

Table 1 Nonlinear model's parameters

Symbol	Definition	Value	Unit
v_y, v_x	Lateral and longitudinal velocities	30	km/h
T	Track width	1.53	m
l_F, l_R	Front and rear wheel distance to COG	1.26 and 1.9	m
m	Vehicle mass	2023	kg
I_z	Yaw inertia	6286	kg m^2

$$I_z\dot{\gamma} = l_f\big((F_{yFL} + F_{yFR})\cos\delta + (F_{xFL} + F_{xFR})\sin\delta\big) - l_r(F_{yRL} + F_{yRR}) + \frac{T}{2}\big((-F_{xFL} + F_{xFR})\cos\delta + (F_{yFL} - F_{yFR})\sin\delta - F_{xRL} + F_{xRR}\big) \tag{3}$$

where F_{xi} and $F_{yi}(i = \text{FR, FL, RR, RL})$ denote the longitudinal and lateral forces of each tyre and γ indicates the yaw rate. The model comprises dynamic load transfer for generation of normal force. The equations are as follows:

$$F_{zFL,FR} = mg\frac{l_r}{2(l_f + l_r)} - ma_x\frac{h}{2(l_f + l_r)} \mp \frac{ma_y}{2T} \tag{4}$$

$$F_{zRL,RR} = mg\frac{l_f}{2(l_f + l_r)} + ma_x\frac{h}{2(l_f + l_r)} \mp \frac{ma_y}{2T} \tag{5}$$

where g, a_x and a_y are denoted as the gravitational, longitudinal and lateral acceleration, respectively. The vehicle model also includes nonlinear wheel model where the information concerning the equations can be found in [26].

Fig. 2 Nonlinear vehicle model
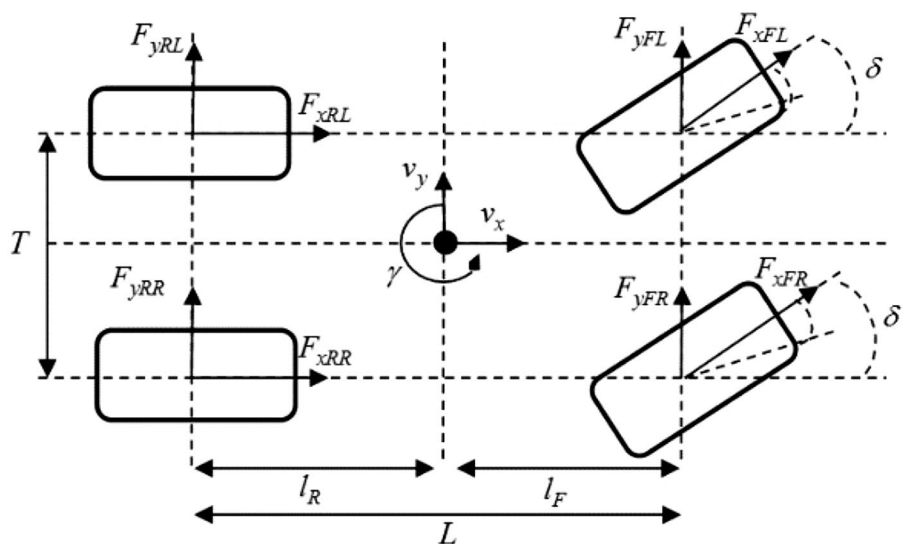
2.2 Stanley controller for path tracking control system

The purpose of implementing a path tracking control system is to provide wheel input to the vehicle based on the pre-defined trajectory. In this study, Stanley controller is selected to fulfil this purpose. The Stanley's control law is given as [27, 28]:

$$\delta_s(t) = \emptyset_e + \tan^{-1}\left(\frac{k_s e(t)}{v(t)}\right) \tag{6}$$

where $\delta_s(t)$ is the wheel angle, $v(t)$ is the vehicle speed and $\emptyset_e$ is the heading error between the pre-defined trajectory direction and vehicle direction of motion, calculated from the difference between yaw angle of the vehicle and trajectory, $\emptyset_e = \varphi - \varphi_{ref}$. k_s is the gain parameter, and e is the lateral error, measured from the centre of front axle to the nearest trajectory point.

3 Proposed lateral control structure

3.1 Proposed control structure

Figure 3 illustrates the structure of the proposed lateral control strategy. The outer loop consists of path tracking system where Stanley controller is applied to track the desired coordinates, x_{ref}, y_{ref}, and heading, φ_{ref}. Stanley controller produces wheel angle, δ_s, from the information of lateral error, e, which is calculated from the desired coordinates, x_{ref}, y_{ref}, and current vehicle coordinates, x_c, y_c, and heading error, $\emptyset_e$, which is calculated from the desired heading, φ_{ref}, and the current heading, φ, of the vehicle. The main

contribution of this study is the inner-loop system which is marked by the grey-coloured box. The purpose is to generate an additional corrective wheel angle, δ_c, to reduce lateral acceleration, a_y. The corrective wheel angle, δ_c, is obtained via fuzzy logic controller (FLC) controller based on the information of the error, e_H, and derivative error, $\dot{e}_H$, of head roll angle. The error, e_H, is the difference between the driver's head roll angle, θ_{HD}, which represents desired response and passenger's head roll angle, θ_{HP}, which represents the actual response. The head roll angles of the driver, θ_{HD}, and passenger, θ_{HP}, are predicted using RBFN modelling method, whereas the input for the RBFN model is the lateral acceleration, a_y. Finally, the wheel angle calculated from the Stanley controller, δ_s, and corrective wheel angle from the FLC controller, δ_c, are combined to be the total wheel input, δ, for the vehicle.

3.2 Radial basis function network modelling and experimental setup

In this study, RBFN modelling method is adopted to developed driver's and passenger's head roll estimator models. The modelling process is based on the correlation of the vehicle lateral acceleration and occupant's head roll angle. The models are expected to produce predicted responses of the head roll angle based on the given lateral acceleration. Figure 4 shows the overview of the RBFN model. It should be noted that the models for the driver and passenger were developed separately. RBFN consists of an input layer with a single input vector, a nonlinear hidden layer with Gaussian RBF and a linear output layer. The input, x, for the model was the lateral acceleration, a_y. The output, y, was the estimated head roll angle responses of the driver, θ_{HD}, or the passenger, θ_{HP}.
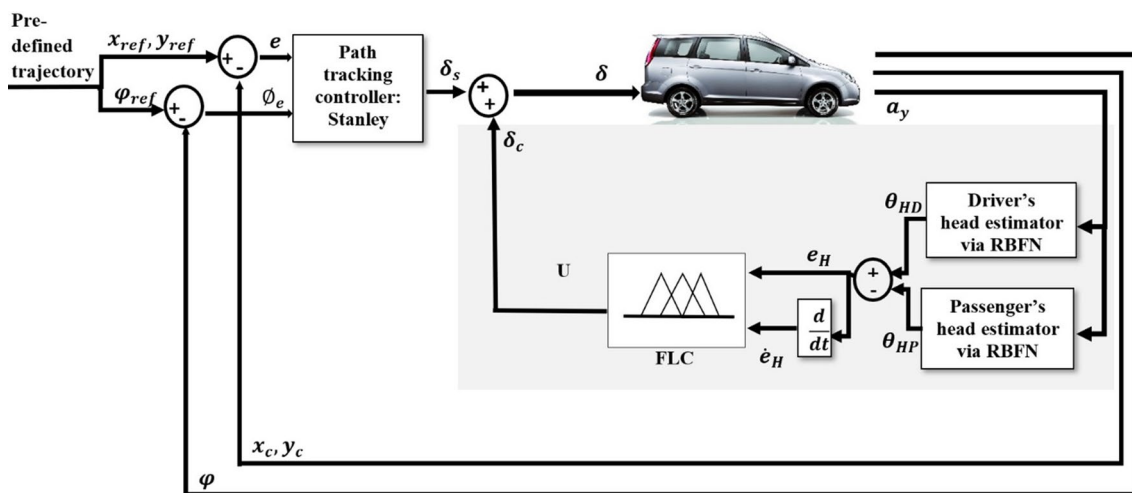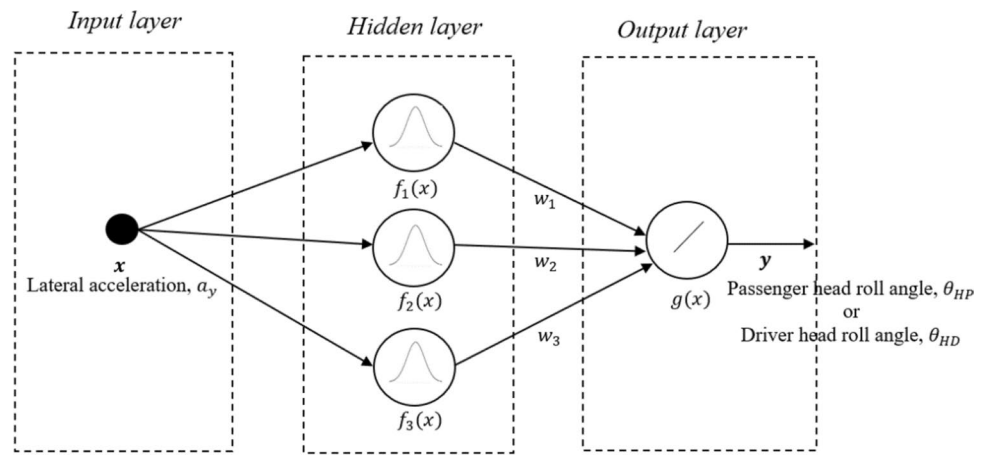

Fig. 3 The structure of the proposed lateral control strategy

Fig. 4 Structure of RBFN model

Based on the Kolmogorov theorem, the number of hidden neurons is determined using the $2n + 1$ formula, where n is equal to the number of inputs [29]. So, the number of hidden neurons which was used in this study is 3. The equation of the Gaussian function in the hidden layer can be expressed as [30–32]:

$$f(x) = \exp\left(\frac{-x - c_j^2}{\sigma^2}\right) \tag{7}$$

where c is the centre point and σ is the RBFN spread. Considering the Gaussian function in (7), the output of the network can be defined as:

$$y = g\left(\sum_{j=1}^{3} w_j \exp\left(\frac{-x - c_j^2}{\sigma^2}\right) + b_2\right) \tag{8}$$

where w is the weight.

Experiment is conducted to gather real-time data of the occupant's head roll angles and lateral acceleration during slalom driving for the modelling process. The experiment which considers MS provocation was set up based on the previous research works from Wada et al. [7]. A multi-purpose vehicle (MPV) is used to perform the data acquisition. The MPV was equipped by several equipment and sensors as depicted in Table 2. Meanwhile, Fig. 5 shows the location of each equipment as given in Table 2.

The experiment was set up by arranging six cones in a straight line on 150-m road. The gap for each cone was set

to 20 m. Figure 6 illustrates the schematic of the test track. Ten adults participated as both the driver and passenger regardless of their gender, ages and skills. The driver's role is to drive in a slalom driving style through the cones at a constant velocity of 30 km/h. The nominal frequency of the lateral acceleration for this customized test track was 0.21 Hz, a frequency that provokes MS. On the other hand, the passenger's role is to act naturally with the tilting movement and avoid any intentional action to move opposite with the typical head tilt movement. Each participant participated as driver and passenger for three times per role. All data were recorded to be used in the modelling process.

3.3 Motion sickness incidence quantification

The most important thing to be measured in this study is the amount of motion sickness incidence (MSI) felt by the passenger. MSI is defined as an index of the severity of MS [9]. The MSI value is quantified using the 6-degree-of-freedom (DOF) subjective vertical conflict (SVC) model which described by Wada et al. [7, 9]. Here, the model is used to calculate the MSI of the passenger by using the information of head roll angle and lateral acceleration. The structure of 6-DOF SVC model is shown in Fig. 7. Details of the configuration can be found in [7, 9]. In this study, the MSI before and after the proposed lateral control system is applied is calculated and compared to investigate the efficiency of the proposed control structure.

Table 2 Details of the equipment

Type	Function	Location
Dewesoft	Data acquisition module	Vehicle's boot
Monitor	Data monitoring	Behind passenger's seat
MTi-G sensor (Xsense Technologies)	Data measuring	Approximate location of vehicle center of gravity (COG) and participant's caps

Fig. 5 Location of the equipment during the experiment

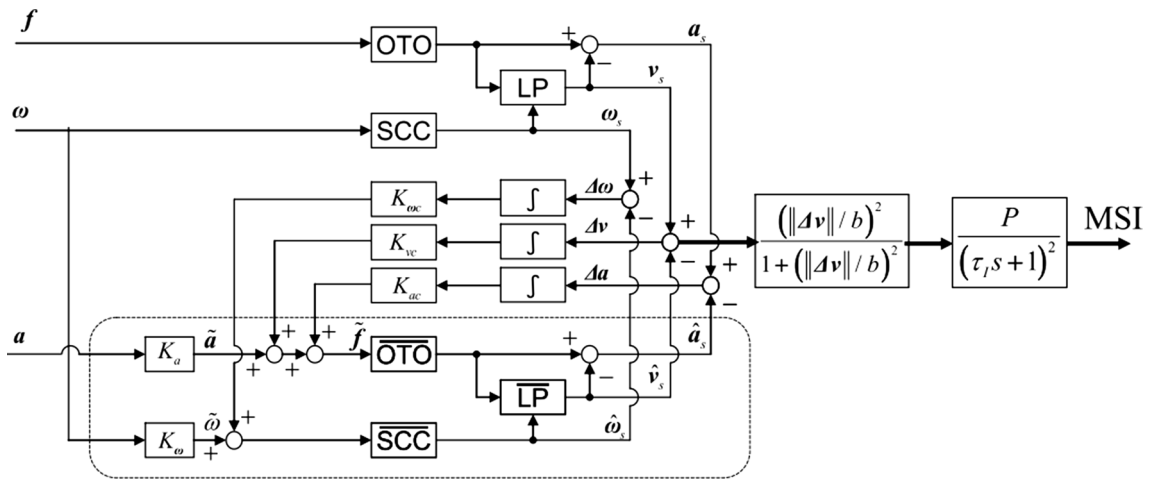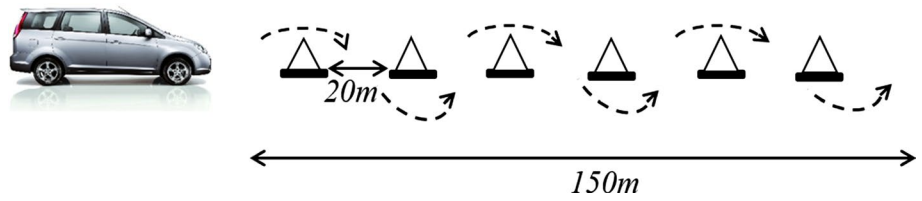**Fig. 6** Schematic of the test track

Fig. 7 Six-DOF SVC model [7]

4 Simulation setup, results and analysis

4.1 Selection of Stanley gain parameter

$$
\delta_s(t) = \begin{cases} \delta_{\max} & \text{if } \emptyset + \tan^{-1}\left(\frac{k_s e(t)}{v(t)}\right) \geq \delta_{\max} \\ \emptyset + \tan^{-1}\left(\frac{ke(t)}{v(t)}\right) & \text{if } \left|\emptyset + \tan^{-1}\left(\frac{k_s e(t)}{v(t)}\right)\right| < \delta_{\max} \\ -\delta_{\max} & \text{if } \emptyset + \tan^{-1}\left(\frac{k_s e(t)}{v(t)}\right) \leq \delta_{\max} \end{cases} \quad (9)
$$

First and foremost, it is crucial to select the suitable gain for Stanley controller as it determines the performance of the vehicle's path tracking. The gain, k_s, is selected based on the following control law [28]: where $\delta_{\max}$ was fixed to be 17°, the maximum degree of the wheel angle of the vehicle which had been used during the experiment. According to the saturation limit in (9), the value of gain k_s in this study is 4.3.

4.2 Fuzzy logic controller configuration

Generally, the membership function and rules of the FLC are selected heuristically based on the designer's experience [33]. As shown in Fig. 8, FLC consists of two inputs and single output membership functions. The first input for FLC is the error of the head roll angle, e_H, which is calculated from the desired/driver's head roll angle, θ_{HD}, and actual/passenger's head roll angle, θ_{HP}. The second input inserted to the FLC is the derivative of the head roll angle error, $\dot{e}_H$. The input variables have been decomposed into three different fuzzy linguistic levels which are Negative (N), Zero (Z) and Positive (P). The control rules are designed in a form of IF–THEN structure which is described in Table 3. Figure 9 shows the control surface of this control scheme.

4.3 Proportional–integral with particle swarm optimization

A PID controller is chosen to be applied in the proposed control structure for comparison purpose with the FLC. The structure of the PID controller is shown in Fig. 10. The input for PID is error of the head roll angle, e_H while the output is corrective wheel angle, δ_c. Here, the PID gain parameters are tuned by using particle swarm optimization (PSO) method. It has been reported that using PSO is less time consuming than using a trial-and-error method [34]. As the aim of the control strategy is to reduce the lateral acceleration, the fitness function of the PSO is defined as the root-mean-squared (RMS) value of the lateral acceleration. The PSO finds optimal PID gain parameters, K_p, K_i, K_d by minimizing the fitness function. The equation of the fitness function is given by:

$$
\text{Fitness function} = f\left(K_p, K_i, K_d\right) = \sqrt{\frac{\sum[a_y(t)]^2}{n_f}} \quad (10)
$$

where a_y is the lateral acceleration and n_f is the number of data.

PSO algorithm works based on the behaviour of agents moving in swarms to find the optimum solution to the imposed optimization problem. The particles of the initial swarm population start with random positions and velocities within the multi-dimensional search space. The particles have the memories of their own best position p_{best} and the overall swarm best position g_{best} based on the optimum fitness value. The determination of the particle's motion for the next position is determined based on the memories. The next position $x_{id}(t + 1)$ and the next velocity $v_{pso}(t + 1)$ are obtained by the following equations:

$$
x_{id}(t + 1) = x_{id}(t) + v_{pso}(t + 1) \quad (11)
$$

$$
\begin{aligned} v_{pso}(t + 1) = {} & iw_{pso} \times v_{pso}(t) + c_{pso} \times \text{rand}(0, 1) \times \left(p_{best}(t) - x_{id}(t)\right) \\ & + s_{pso} \times \text{rand}(0, 1) \times \left(g_{best}(t) - x_{id}(t)\right) \end{aligned} \quad (12)
$$

where iw_{pso} is the inertial weight, c_{pso} is the cognitive coefficient, and s_{pso} is the social coefficient. Over several iterations, the average fitness will be improved. Then, the solution will be converged and the fittest candidates will be found.

Table 4 gives the PSO parameters. The selection of the parameter is adopted from [35]. After going through the optimization process, the value for each gain is determined as: $K_p = -0.003$, $K_i = 0.06$ and $K_d = -0.8$.

4.4 Head roll prediction model by radial basis function network

In this study, the most important outcome of the modelling process is the generalization ability of the model. To test the generalization ability, data from driver's and passenger's data collection are extracted and excluded from the training process. These data are labelled as unseen data. Then, the unseen data are compared with the predicted data produced by the model in the testing process. During the training process, the procedure of adding the spread value, training and testing was repeated until saturated generalization results were obtained. Details of the procedure can be referred in [36]. Through the process, the driver's model starts to saturate when the spread value is 1.6, while the passenger's model starts to saturate when the spread value is 2.1. The generalization responses of the driver's and passenger's models when their spread values were 1.6 and 2.1 are shown in Fig. 11. The saturated

Fig. 8 Membership functions of input–output in FLC

(a) Membership function of input e_H

(b) Membership function of input $\dot{e}_H$

(c) Membership function of output U
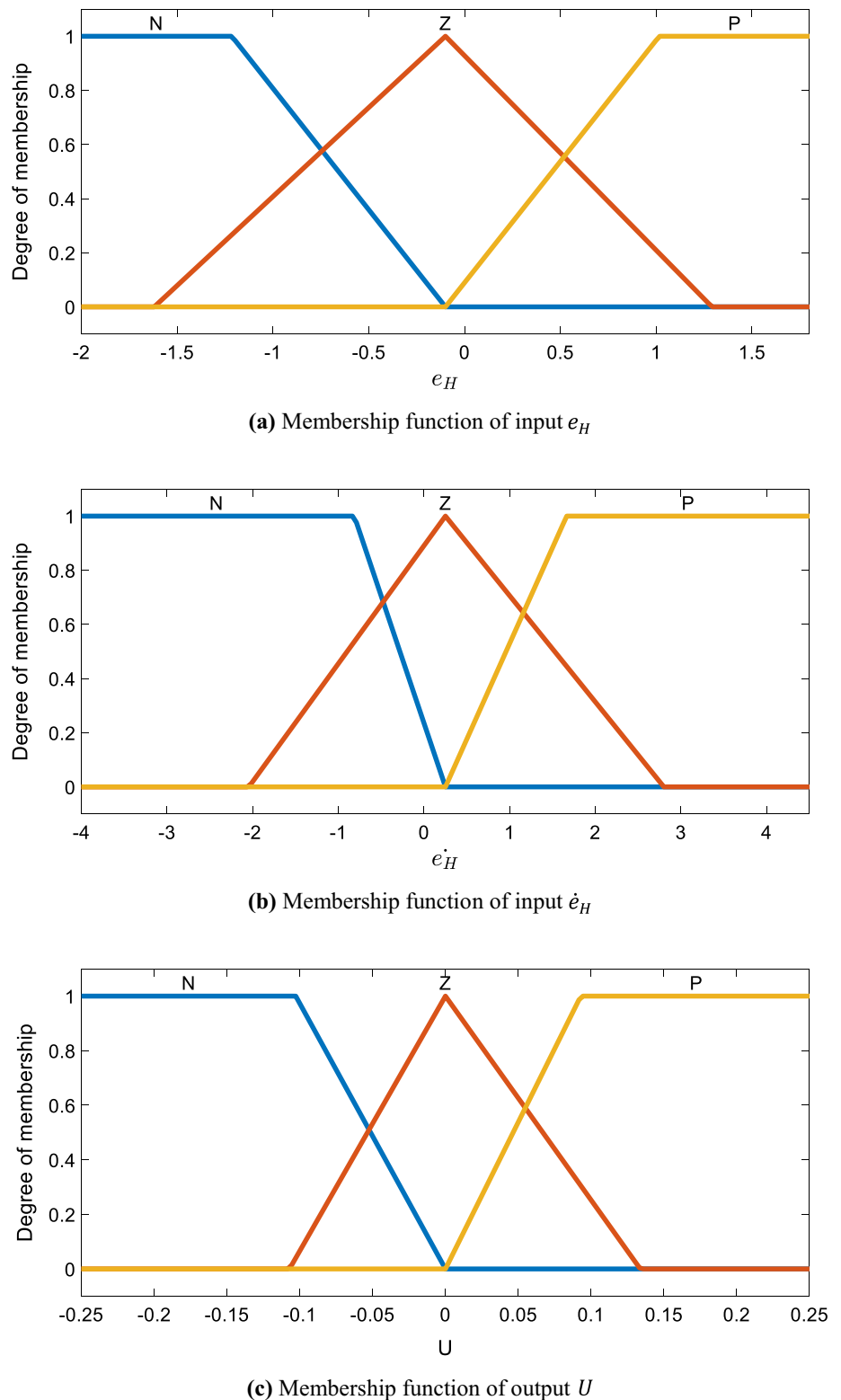
generalization results were assumed to be an indicator to determine that the spread value was already ample. Here, the models with spread value 1.6 and 2.1 are selected as the best driver's and passenger's models to be applied in

the proposed control structure. In addition, the regression value for both models are 92.08% and 90.15%. Regression represents the strength of a linear relationship between the real data output and the predicted output.

Table 3 Fuzzy rules

$\dot{e}_H$ \ e_H	N	Z	P
N	P	P	P
Z	Z	Z	Z
P	N	N	N
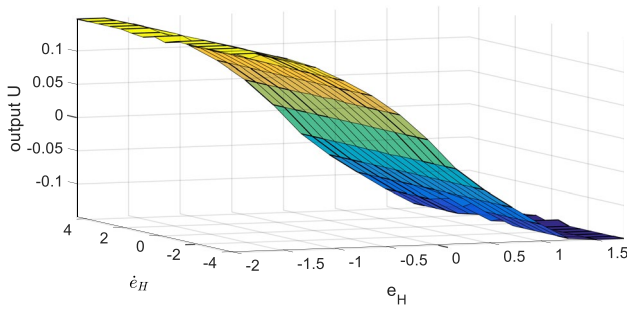
Fig. 9 Control surface of the FLC
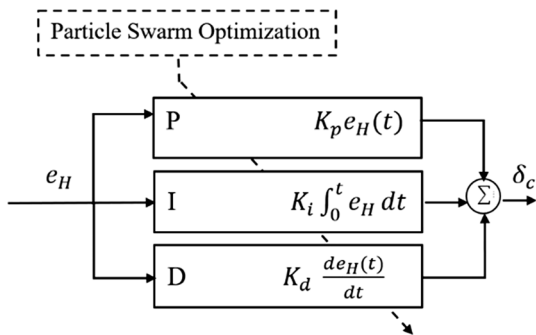
Fig. 10 The structure of PID controller

Table 4 PSO parameters

Parameters	Value
Cognitive coefficient, c_{pso}	1.42
Social coefficient, s_{pso}	1.42
Inertial weight, iw_{pso}	0.9
Number of variables (dimension), N_d	3 (K_p, K_i, K_d)
Upper bound limit	[−0.001, 0.08, −0.2]
Lower bound limit	[−0.005, 0.03, −0.8]
Number of particles, N_p	50
Number of iterations, N_i	20

Based on Eqs. (7) and (8), the value of the centre point c, spread σ and weight w for the driver's and passenger's model are as follows:

Driver's model:

$$c = \begin{bmatrix} -2.5560 \\ 3.6721 \\ -0.6546 \end{bmatrix} \sigma = \begin{bmatrix} 1.6 \\ 1.6 \\ 1.6 \end{bmatrix} w = \begin{bmatrix} 8.6564 \\ -8.5897 \\ 0.8409 \end{bmatrix} \quad (13)$$

Passenger's model:

$$c = \begin{bmatrix} -3.9402 \\ 3.7988 \\ -3.6039 \end{bmatrix} \sigma = \begin{bmatrix} 2.1 \\ 2.1 \\ 2.1 \end{bmatrix} w = \begin{bmatrix} 14.5623 \\ 11.6248 \\ -26.7979 \end{bmatrix} \quad (14)$$

4.5 Evaluation of the proposed control strategy

The proposed control strategy is evaluated via Matlab/ Simulink simulations. The vehicle runs at a constant speed of 30 km/h, according to the pre-defined trajectory which is taken from the previously conducted experiment. The trajectory is illustrated in Fig. 12. Every curve along the path is characterized by Curve 1 up to Curve 6 to enable an easier understanding of the simulation results. The simulation is carried out in three different situations: (1) Inner-loop system is not included in the overall control structure, (2) inner-loop system with PID controller is included in the overall control structure, and (3) inner-loop system with FLC is included in the overall control structure.

In the evaluation process, results of lateral acceleration, passenger's head roll angle and MSI are recorded and analysed. Figure 13a shows the responses of the lateral acceleration for every situation. Meanwhile, Fig. 13b displays the findings of the maximum lateral acceleration for every curve in graphical form. The results show that the maximum lateral acceleration response had declined in every curve. This indicated that the proposed control strategy succeeded in achieving the objective which was to reduce the lateral acceleration during curve driving. The purpose of observing the maximum lateral acceleration value was to determine the extent of decrease once the vehicle has attained at peak cornering. Based on the results in Fig. 13, FLC managed to reduce more lateral acceleration than the PID.

Figure 14a shows the responses of the passenger's head roll angle, while Fig. 14b shows the numerical results of the maximum passenger's head roll angle for each curve. Similar to the lateral acceleration results, the head roll angle is reduced when the proposed control strategy is applied. Also, FLC managed to reduce more head roll angle than the PID. Although an oscillatory behaviour occurs in the beginning of lateral acceleration and head roll responses for FLC-based system, the oscillation responses are considered small and do not give significant effect to MS. This is due to the MSI calculation which is based on the overall responses.

Fig. 11 Generalization responses of driver's and passenger's models
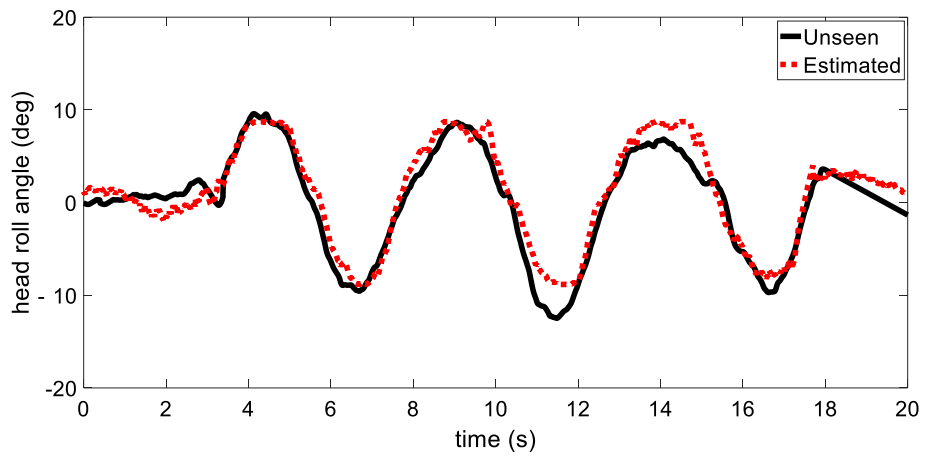
(a) Generalization response of driver's model when the spread value is 1.6
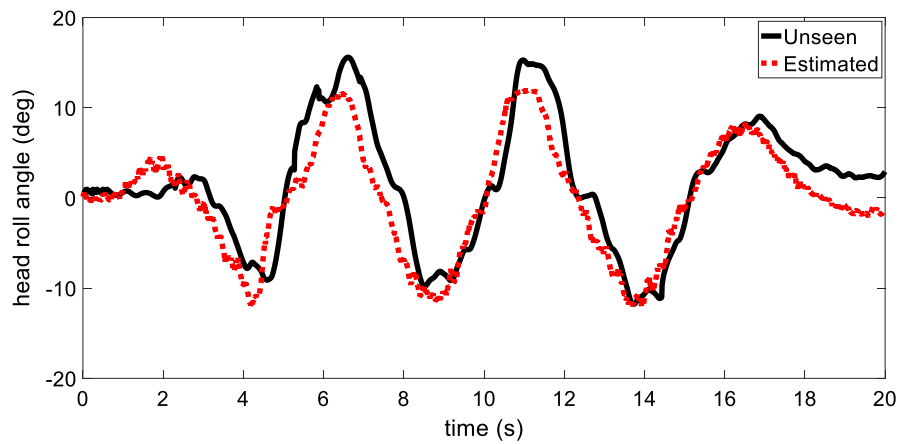
(b) Generalization response of passenger's model when the spread value is 2.1

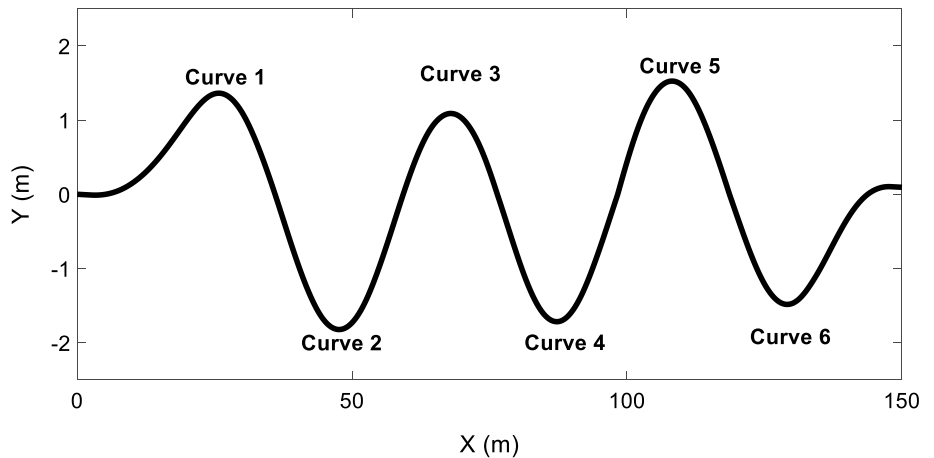**Fig. 12** Pre-defined trajectory

Figure 15 depicts the findings of the MSI. The pre-defined trajectory that is illustrated in Fig. 12 is referred to as 1 lap. In order to investigate the MSI value when the time was increased, the simulation was continued for 10 laps. Table 5 gives the analysis of the MSI. FLC produced the biggest percentage of reduction among all which are 3.25% in single lap and 10.86% in 10 laps. Based on the analysis, the MSI gap of all situations expanded following the extension of the time.

Fig. 13 Lateral acceleration results
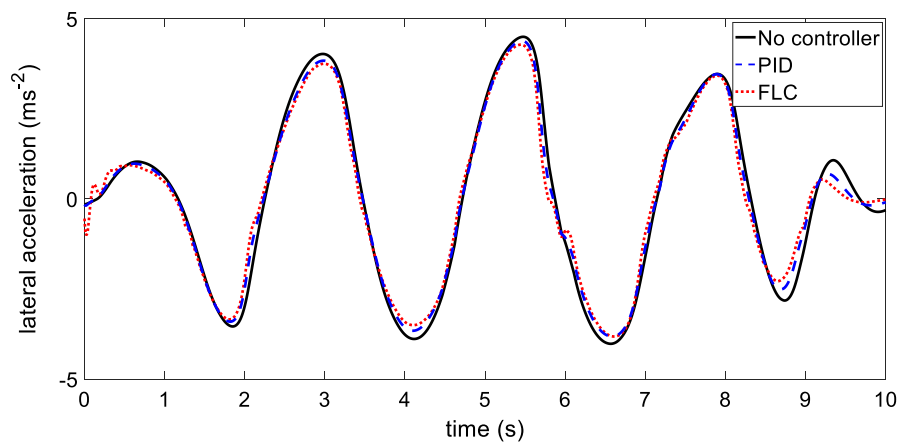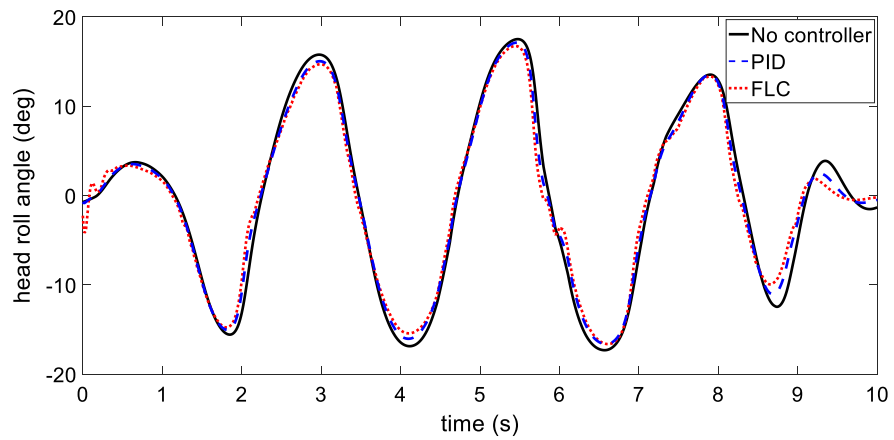

(a) Responses of lateral acceleration
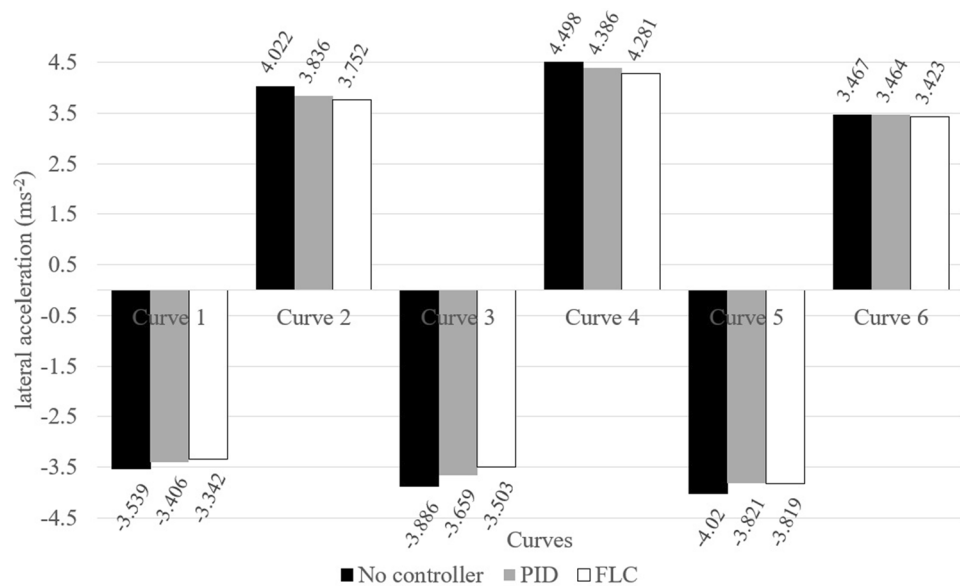
(b) Numerical results of the maximum lateral acceleration for each curve

This finding was in agreement with the previous studies by Wada et al. where the difference of MSI between driver's and passenger's increased as the time elapsed [9]. Therefore, it is expected that the MSI reduction will keep increasing if the simulation time increases. It means that the proposed control structure is significant to reduce the MS experienced by the passengers especially when the time elapses. These findings indicated that the recommended control approach was useful in reducing the quantity of the passenger's MSI during slalom manoeuvre.

5 Conclusions and future works

MS occurred due to the high lateral acceleration that resulted from inappropriate wheel's turning. The high lateral acceleration causes a bigger passenger's head roll angle towards the lateral acceleration direction during cornering. In this situation, the percentage of MSI is high. Thus, this study proposed a lateral control strategy to generate an additional corrective wheel angle to reduce the

Fig. 14 Passenger's head roll angle


(a) Responses of head roll angle
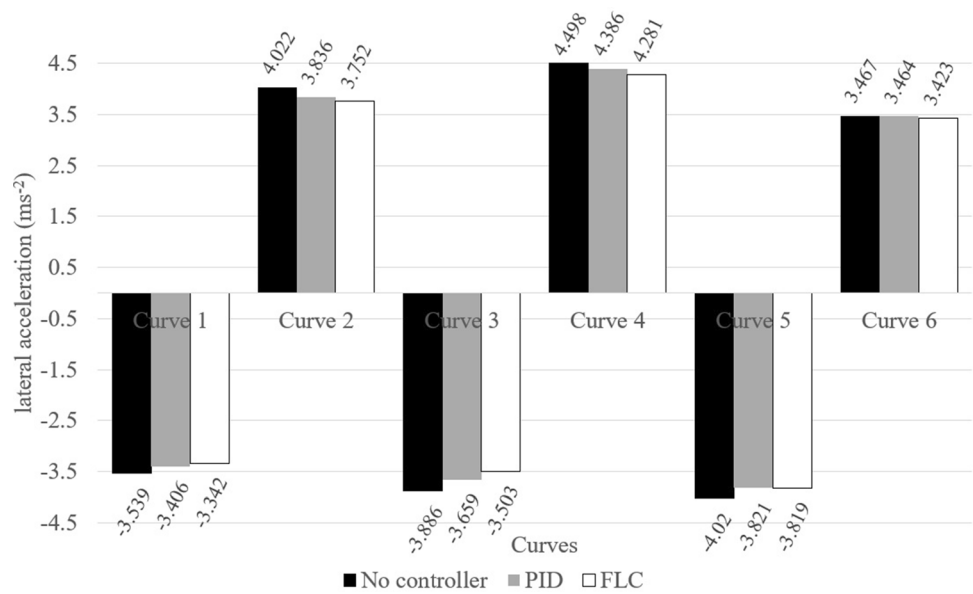
**(b)** Numerical results of the maximum head roll angle for each curve

lateral acceleration as well as the passenger's head roll angle so that the MSI can be minimized. The main contribution of this study is by introducing a new controlled variable which is head roll angle to produce the corrective wheel angle. The idea is originated by the correlation of vehicle lateral acceleration and the occupant's head roll movement during curvature. The proposed control strategy with FLC managed to improve the MSI by 3.25% in a single lap and 10.86% in 10 laps, compared to PID controller which managed to improve the MSI by only 2.18% in a single lap and 6.91% in 10 laps. For the time being, due to the limited budget and equipment, the evaluation is only done through simulation platform. In future, it is necessary to investigate the effectiveness of the control structure in real time using an autonomous vehicle.

Fig. 15 Results of MSI
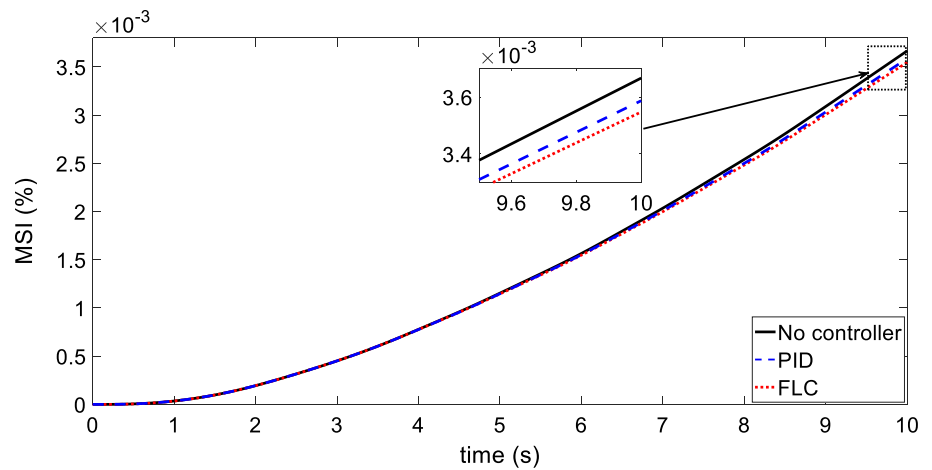
(a) MSI for 1 lap
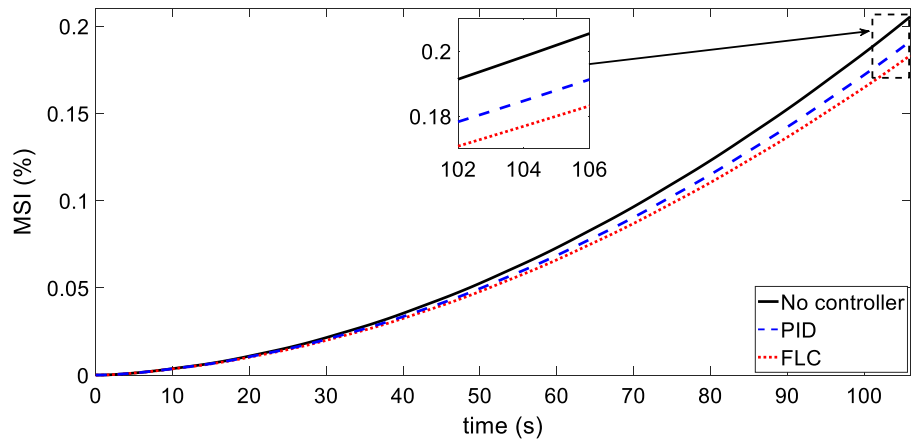
(b) MSI for 10 laps

Table 5 Analysis of MSI

	MSI (%)		Reduction (%)	
	1 lap	10 laps	1 lap	10 laps
No controller	0.003667	0.2054	–	–
PID	0.003587	0.1912	2.18	6.91
FLC	0.003548	0.1831	3.25	10.86

References

1. Tian D, Wu G, Boriboonsomsin K, Barth MJ (2017) A co-benefit and tradeoff evaluation framework for connected and automated vehicle applications. In: 2017 IEEE intelligent vehicles symposium (IV), pp 953–958

2. Diels C (2014) Will autonomous vehicles make us sick? In: Sharples S, Shorrock S (eds) Contemporary ergonomics and human factors. Taylor & Francis, Routledge, pp 301–307

3. Kennedy RS, Drexler J, Kennedy RC (2010) Research in visually induced motion sickness. Appl Ergon 41:494–503

4. Diels C, Bos JE (2015) User interface considerations to prevent self-driving carsickness. In: Adjunct proceedings of the 7th international conference on automotive user interfaces and interactive vehicular applications, pp 14–19

5. Green P (2016) Motion sickness and concerns for self-driving vehicles: a literature review. Technical report UMTRI-2016, University of Michigan Transportation Research Institute, pp 1–83

6. Wada T, Konno H, Fujisawa S, Doi S (2012) Can passengers' active head tilt decrease the severity of carsickness?: Effect of head tilt on severity of motion sickness in a lateral acceleration environment. Hum Factors 54(2):226–234

7. Wada T, Kamiji N, Doi S (2013) A mathematical model of motion sickness in 6DOF motion and its application to vehicle passengers. In: 2nd international conference on digital human modeling, pp 1–6

8. Wada T, Fujisawa S, Imaizumi K, Kamiji N, Doi S (2010) Effect of driver's head tilt strategy on motion sickness incidence. IFAC Proc 43(13):192–197

9. Wada T, Fujisawa S, Doi S (2018) Analysis of driver's head tilt using a mathematical model of motion sickness. Int J Ind Ergon 63:89–97

10. Turner M, Griffin MJ (1999) Motion sickness in public road transport: the effect of driver, route and vehicle. Ergonomics 42(12):1646–1664

11. Elbanhawi M, Simic M, Jazar R (2015) In the passenger seat: investigating ride comfort measures in autonomous cars. IEEE Intell Transp Syst Mag 7(3):4–17

12. Utbult J (2017) A study on low-speed maneuverability and highway lateral comfort. Master thesis, Chalmers University of Technology

13. Saruchi S'A, Zamzuri H, Zulkarnain N, Mohammed Ariff MH, Wahid N (2017) Composite nonlinear feedback with disturbance observer for active front steering. Indones J Electr Eng Comput Sci 7(2):434–441

14. Aripin MK, Sam Y, Danapalasingam KA, Peng K, Hamzah N, Ismail MF (2014) A review of active yaw control system for vehicle handling and stability enhancement. Int J Veh Technol 2014:1–16

15. Shahrieel M, Aras M, Wahyuddin M, Azmi N, Kamaruddin MN (2017) A study of tuning process of fuzzy logic controller output membership function for AUV-pitch control. In: 2017 IEEE 7th international conference on underwater system technology: theory and applications (USYS), pp 1–5

16. Kumar S, Nagpal P (2017) Comparative analysis of P, PI, PID and fuzzy logic controller for tank water level control system. Int Res J Eng Technol 4(4):1174–1177

17. Londhe PS, Santhakumar M, Patre BM, Member S, Waghmare LM (2017) Task space control of an autonomous underwater vehicle manipulator system by robust single-input fuzzy logic control scheme. IEEE J Ocean Eng 42(1):13–28

18. Saruchi S'A, Zamzuri H, Hassan N, Mohammed Ariff MH (2018) Modeling of head movements towards lateral acceleration direction via system identification for motion sickness study. In: International conference on information and communications technology (ICOIACT), pp 633–638

19. Saruchi S'A, Zamzuri H, Mohammed Ariff MH, Hassan N (2018) Modelling of occupant's head tilt movement in motion sickness study using Hammerstein–Wiener system. In: Proceedings of 7th international graduate conference on engineering, science & humanities, August 2018, pp 25–27

20. Saruchi S'A, Mohammed Ariff MH, Zamzuri H, Hassan N, Wahid N (2018) Artificial neural network for modelling of the correlation between lateral acceleration and head movement in a motion sickness study. IET Intel Transport Syst 13(2):340–346

21. Saruchi S'A, Mohammed Ariff MH, Zamzuri H, Hassan N, Wahid N (2019) Modeling of occupant's head movement behavior in motion sickness study via time delay neural network. Simulation 96(2):131–140

22. Zheng J, Suzuki K, Fujita M (2013) Car-following behavior with instantaneous driver-vehicle reaction delay: a neural-network-based methodology. Transp Res Part C Emerg Technol 36:339–351

23. Yang S, Ting TO, Man KL, Guan S (2013) Investigation of neural networks for function approximation. Procedia Comput Sci 17:586–594

24. Zhu JZ, Cao JX, Zhu Y (2014) Traffic volume forecasting based on radial basis function neural network with the consideration of traffic flows at the adjacent intersections. Transp Res Part C Emerg Technol 47:139–154

25. Osborn RP, Shim T (2006) Independent control of all-wheel-drive torque distribution. Veh Syst Dyn 44(7):529–546

26. Nagai M, Shino M, Gao F (2002) Study on integrated control of active front steer angle and direct yaw moment. JSAE Rev 23(3):309–315

27. Thrun S et al (2006) Stanley: the robot that won the DARPA grand challenge. J F Robot 23(9):245–267

28. Hoffmann GM, Tomlin CJ, Montemerlo M, Thrun S (2007) Autonomous automobile trajectory tracking for off-road driving: controller design, experimental validation and racing. In: 2007 American control conference, pp 2296–2301

29. Hecht-Nielsen R (1989) Theory of the backpropagation neural network. In: International 1989 joint conference on neural networks, vol 1, pp 593–605

30. Awad M, Qasrawi I (2016) Enhanced RBF neural network model for time series prediction of solar cells panel depending on climate conditions (temperature and irradiance). Neural Comput Appl 30(6):1757–1768

31. Chen D (2017) Research on traffic flow prediction in the big data environment based on the improved RBF neural network. IEEE Trans Ind Inform 13(4):2000–2008

32. Wang G et al (2018) Application of the radial basis function neural network to the short term prediction of the Earth's polar motion. Stud Geophys Geod 62:2017

33. Kim JY, Kim HM, Kim SK, Jeon JH, Choi HK (2011) Designing an energy storage system fuzzy PID controller for microgrid islanded operation. Energies 4(9):1443–1460

34. Jamin NF, Abdul Ghani N (2016) Two-wheeled wheelchair stabilization control using fuzzy logic controller based particle swarm optimization. In: 2016 IEEE international conference on automatic control and intelligent systems (I2CACIS), pp 180–185

35. Khairuddin IM et al (2014) Modeling and simulation of swarm intelligence algorithms for parameters tuning of PID controller in industrial couple tank system. Adv Mater Res 903:321–326

36. Saruchi S'A et al (2019) Radial basis function neural network for head roll prediction modelling in a motion sickness study. Indones J Electr Eng Comput Sci 15(3):1637–1644